Hindawi Publishing Corporation
EURASIP Journal on Image and Video Processing
Volume 2008, Article ID 528297, 11 pages
doi:10.1155/2008/528297

Research Article

Efficient Adaptive Combination of Histograms for Real-Time Tracking

F. Bajramovic,[1] B. Deutsch,[2] Ch. Gräßl,[2] and J. Denzler[1]

[1] *Department of Mathematics and Computer Science, Friedrich-Schiller University Jena, 07737 Jena, Germany*
[2] *Computer Science Department 5, University of Erlangen-Nuremberg, 91058 Erlangen, Germany*

Correspondence should be addressed to F. Bajramovic, ferid.bajramovic@informatik.uni-jena.de

Received 30 October 2007; Revised 14 March 2008; Accepted 12 July 2008

Recommended by Fatih Porikli

We quantitatively compare two template-based tracking algorithms, Hager's method and the hyperplane tracker, and three histogram-based methods, the mean-shift tracker, two trust-region trackers, and the CONDENSATION tracker. We perform systematic experiments on large test sequences available to the public. As a second contribution, we present an extension to the promising first two histogram-based trackers: a framework which uses a weighted combination of more than one feature histogram for tracking. We also suggest three weight adaptation mechanisms, which adjust the feature weights during tracking. The resulting new algorithms are included in the quantitative evaluation. All algorithms are able to track a moving object on moving background in real time on standard PC hardware.

1. INTRODUCTION

Data driven, real-time object tracking, is still an important and in general unsolved problem with respect to robustness in natural scenes. For many high-level tasks in computer vision, it is necessary to track a moving object—in many cases on moving background—in real time without having specific knowledge about its 2D or 3D structure. Examples are surveillance tasks, action recognition, navigation of autonomous robots, and so forth. Usually, tracking is initialized based on change detection in the scene. From this moment on, the position of the moving target is identified in each consecutive frame.

Recently, two promising classes of 2D data-driven tracking methods have been proposed: template- (or region-) based tracking methods and histogram-based methods. The idea of template-based tracking consists of defining a region of pixels belonging to the object and using local optimization methods to estimate the transformation parameters of the region between two consecutive images. Histogram-based methods represent the object by a distinctive histogram, for example, a color histogram. They perform tracking by searching for a region in the image whose histogram best matches the object histogram from the first image. The search is typically formulated as a nonlinear optimization problem.

As the first contribution of this paper, we present a comparative evaluation (previously published at a conference [1]) of five different object trackers, two template-based [2, 3] and three histogram-based approaches [4–6]. We test the performance of each tracker with pure translation estimation, as well as with translation and scale estimation. Due to the rotational invariance of the histogram-based methods, further motion models, such as rotation or general affine motion, are not considered. In the evaluation, we focus especially on natural scenes with changing illuminations and partial occlusions based on a publicly available dataset [7].

The second contribution of this paper concentrates on the promising class of histogram-based methods. We present an extension of the mean-shift and trust-region trackers, which allows using a weighted combination of several different histograms (previously published at a conference [8]). We refer to this new tracker as *combined histogram tracker* (CHT). We formulate the tracking optimization problem in a general way such that the mean-shift [9] as well as the trust-region [10] optimization can be applied. This allows for a maximally flexible choice of the parameters which

are estimated during tracking, for example, translation, and scale.

We also suggest three different online weight adaptation mechanisms for the CHT, which automatically adapt the weights of the individual features during tracking. We compare the CHT (with and without weight adaptation) with histogram trackers using only one specific histogram. The results show that the CHT with constant weights can improve the tracking performance when good weights are chosen. The CHT with weight adaptation gives good results *without* a need for a good choice for the right feature or optimal feature weights. All algorithms run in real time (up to 1000 frames per second excluding IO).

The paper is structured as follows: In Section 2, we give a short introduction to template-based tracking. Section 3 gives a more detailed description of histogram-based trackers and shows how two suitable local optimization methods, the mean-shift and trust-region algorithms, can be applied. In Sections 4 and 5, we present the main algorithmic contributions of the paper: a rigorous mathematical description for the CHT followed by the weight adaptation mechanisms. Section 6 presents the experiments: we first describe the test set and evaluation criteria we use for our comparative study. The main comparative contribution of the paper consists of the evaluation of the different tracking algorithms in Section 6.2. In Sections 6.3 and 6.4, we present the results for the CHT and the weight adaptation mechanisms. The paper concludes with a discussion and an outlook to future work.

2. REGION-BASED OBJECT TRACKING USING TEMPLATES

One class of data driven object tracking algorithms is based on template matching. The object to be tracked is defined by a *reference region* $\mathbf{r} = (\mathbf{u}_1, \mathbf{u}_2, \ldots, \mathbf{u}_M)^T$ in the first image. The gray-level intensity of a point $\mathbf{u}$ at time t is given by $f(\mathbf{u}, t)$. Accordingly, the vector $\mathbf{f}(\mathbf{r}, t)$ contains the intensities of the entire region $\mathbf{r}$ at time t and is called *template*. During initialization, the *reference template* $\mathbf{f}(\mathbf{r}, 0)$ is extracted from the first image.

Template matching is performed by computing the motion parameters $\boldsymbol{\mu}(t)$ which minimize the squared intensity differences between the reference template and the current template:

$$\boldsymbol{\mu}(t) = \underset{\text{size}\,\boldsymbol{\mu}}{\operatorname{argmin}} \left|\left|\mathbf{f}(\mathbf{r}, 0) - \mathbf{f}(\mathbf{g}(\mathbf{r}, \boldsymbol{\mu}), t)\right|\right|_2. \tag{1}$$

The function $\mathbf{g}(\mathbf{r}, \boldsymbol{\mu})$ defines a geometric transformation of the region, parameterized by the vector $\boldsymbol{\mu}$. Several such transformations can be considered, for example, Jurie and Dhome [3] use translation, rotation, and scale, but also affine and projective transformations. In this paper, we restrict ourselves to translation and scale estimation.

A brute-force search minimization of (1) is computationally expensive. It is more efficient to approximate $\boldsymbol{\mu}$ through a linear system:

$$\hat{\boldsymbol{\mu}}(t+1) = \hat{\boldsymbol{\mu}}(t) + \mathbf{A}(t+1)\left(\mathbf{f}(\mathbf{r}, 0) - \mathbf{f}\left(\mathbf{g}(\mathbf{r}, \hat{\boldsymbol{\mu}}(t)),\, t+1\right)\right). \tag{2}$$

For detailed background information on this class of tracking approaches, the reader is referred to [11].

We compare two approaches for computing the matrix $\mathbf{A}(t+1)$ in (2). Jurie and Dhome [3] perform a short training step, which consists of simulating random transformations of the reference template. The resulting tracker will be called *hyperplane tracker* in our experiments. Typically, around 1000 transformations are executed and their motion parameters $\tilde{\boldsymbol{\mu}}_i$ and difference vectors $\mathbf{f}(\mathbf{r}, 0) - \mathbf{f}(\mathbf{g}(\mathbf{r}, \tilde{\boldsymbol{\mu}}_i), 0)$ are collected. Afterwards, the matrix $\mathbf{A}$ is derived through a least squares approach. Note that this allows making $\mathbf{A}$ independent of t. For details, we refer to the original paper.

Hager and Belhumeur [2] propose a more analytical approach based on a first-order Taylor approximation. During initialization, the gradients of the region points are calculated and used to build a Jacobian matrix. Although $\mathbf{A}$ cannot be made independent of t, the transformation can be performed very efficiently and the approach has real-time capability.

3. REGION-BASED OBJECT TRACKING USING HISTOGRAMS

3.1. Representation and tracking

Another type of data driven tracking algorithms is based on histograms. As before, the object is defined by a reference region, which we denote by $R(\mathbf{x}(t))$, where $\mathbf{x}(t)$ contains the time variant parameters of the region, also referred to as the state of the region. Note that $R(\mathbf{x}(t))$ is similar, but not identical, to $\mathbf{g}(\mathbf{r}, \boldsymbol{\mu}(t))$. The later transforms a set of pixel coordinates to a set of (sub)pixel coordinates, while the former defines a region in the plane, which is implicitly treated as the set of pixel coordinates within that region. This implies that $R(\mathbf{x}(t))$ does not contain any subpixel coordinates. One simple example for a region is a rectangle of fixed dimensions. The state of the region $\mathbf{x}(t) = (m_x(t), m_y(t))^T$ is the center of the rectangle in (sub)pixel coordinates $m_x(t)$ and $m_y(t)$ for each time step t. With this simple model, tracking the translation of a region can be described as estimating $\mathbf{x}(t)$ over time. If the size of the region is also included in the state, estimating the scale will also be possible.

The information contained within the reference region is used to model the moving object. The information may consist of the color, the gray value, or certain other features, like the gradient. At each time step t and for each state $\mathbf{x}(t)$, the representation of the moving object consists of a probability density function $p(\mathbf{x}(t))$ of the chosen features within the region $R(\mathbf{x}(t))$. In practice, this density function has to be estimated from image data. For performance reasons, a weighted histogram $\mathbf{q}(\mathbf{x}(t)) = (q_1(\mathbf{x}(t)), q_2(\mathbf{x}(t)), \ldots, q_N(\mathbf{x}(t)))^T$ of N bins $q_i(\mathbf{x}(t))$ is used as a nonparametric estimate of the true density, although it is well known that this is not the best choice from a theoretical point of view [12]. Each individual bin $q_i(\mathbf{x}(t))$ is computed by

$$q_i(\mathbf{x}(t)) = C_{\mathbf{x}(t)} \sum_{\mathbf{u} \in R(\mathbf{x}(t))} L_{\mathbf{x}(t)}(\mathbf{u}) \delta(b_t(\mathbf{u}) - i), \quad i = 1, \ldots, N, \tag{3}$$

where $L_{\mathbf{x}(t)}(\mathbf{u})$ is a suited weighting function, which will be introduced below, b_t is a function which maps the pixel coordinate $\mathbf{u}$ to the bin index $b_t(\mathbf{u}) \in \{1, \ldots, N\}$ according to the feature at position $\mathbf{u}$, and δ is the Kronecker-Delta function. The value $C_{\mathbf{x}(t)} = 1/\sum_{\mathbf{u}\in R(\mathbf{x}(t))} L_{\mathbf{x}(t)}(\mathbf{u})$ is a normalizing constant. In other words, (3) counts all occurrences of pixels that fall into bin i, where the increment within the sum is given by the weighting function $L_{\mathbf{x}(t)}(\mathbf{u})$.

Object tracking can now be defined as an optimization problem. We initially extract the reference histogram $\mathbf{q}(\mathbf{x}(0))$ from the reference region $R(\mathbf{x}(0))$. For $t > 0$, the tracking problem is defined by

$$\mathbf{x}(t) = \operatorname*{argmin}_{\mathbf{x}} D\big(\mathbf{q}(\mathbf{x}(0)), \mathbf{q}(\mathbf{x})\big), \tag{4}$$

where $D(\cdot, \cdot)$ is a suitable distance function defined on histograms. We use three local optimization techniques: the *mean-shift* algorithm [4, 9], a *second-order trust-region* algorithm [5, 10] (referred to simply as the trust-region tracker), and also a simple *first-order trust-region* variant [13] (called first-order trust-region tracker or trust-region 1st for short), which can be considered as gradient descent with online step size adaptation. It is also possible to apply quasiglobal optimization using a particle filter and the CONDENSATION algorithm as suggested by Pérez et al. [6], and Isard and Blake [14].

3.2. Kernel and distance functions

There are two open aspects left: the choice of the weighting function $L_{\mathbf{x}(t)}(\mathbf{u})$ in (3) and the distance function $D(\cdot, \cdot)$. The weighting function is typically chosen as an elliptic kernel, whose support is exactly the region $R(\mathbf{x}(t))$, which thus has to be an ellipse. Different kernel profiles can be used, for example, the Epanechnikov, the biweight, or the truncated Gauss profile [13].

For the optimization problem in (4), several distance functions on histograms have been proposed, for example, the Bhattacharyya distance, the Kullback-Leibler distance, the Euclidean distance, and calar product-based distance. It is worth noting that for the following optimization no metric is necessary. The main restriction on the given distance functions in our work is the following special form

$$D(\mathbf{q}(\mathbf{x}(0)), \mathbf{q}(\mathbf{x})) = \widetilde{D}\left(\sum_{n=1}^{N} d(q_n(\mathbf{x}(0)), q_n(\mathbf{x}))\right) \tag{5}$$

with a monotonic, bijective function $\widetilde{D}$, and a function $d(a, b)$, which is twice differentiable with respect to b. By substituting (5) into (4), we get

$$\mathbf{x}(t) = \operatorname*{argmax}_{\mathbf{x}} -S(\mathbf{x}) \tag{6}$$

$$\text{with } S(\mathbf{x}) = \operatorname{sgn}(\widetilde{D}) \sum_{n=1}^{N} d(q_n(\mathbf{x}(0)), q_n(\mathbf{x})), \tag{7}$$

where $\operatorname{sgn}(\widetilde{D}) = 1$ if $\widetilde{D}$ is monotonically increasing, and $\operatorname{sgn}(\widetilde{D}) = -1$ if $\widetilde{D}$ is monotonically decreasing. More details can be found in [13]. The following subsections deal with the optimization of (6) using the mean-shift algorithm as well as trust-region optimization.

3.3. Mean-shift optimization

The main idea for the derivation of the mean-shift tracker consists of a first-order Taylor approximation of the mapping $\mathbf{q}(\mathbf{x}) \to -S(\mathbf{x})$ at $\mathbf{q}(\hat{\mathbf{x}})$, where $\hat{\mathbf{x}}$ is the estimate for $\mathbf{x}(t)$ from the previous mean-shift iteration (in the first iteration, the result from frame $t-1$ is used instead). Furthermore, the state $\mathbf{x}$ has to be restricted to the position of the moving object in the image plane (tracking of position only). After a couple of computations and simplifications (for details, see [13]), we get

$$\begin{aligned}\mathbf{x}(t) &\approx \operatorname*{argmax}_{\mathbf{x}} \left(C_0 \sum_{\mathbf{u}\in R(\mathbf{x})} L_{\mathbf{x}}(\mathbf{u}) \sum_{n=1}^{N} \delta\big(b_t(\mathbf{u}) - n\big)\, \widetilde{w}_t(\hat{\mathbf{x}}, n) \right) \\ &= \operatorname*{argmax}_{\mathbf{x}} \left(C_0 \sum_{\mathbf{u}\in R(\mathbf{x})} L_{\mathbf{x}}(\mathbf{u}) \widetilde{w}_t(\hat{\mathbf{x}},\, b_t(\mathbf{u})) \right)\end{aligned} \tag{8}$$

with the weights

$$\widetilde{w}_t(\hat{\mathbf{x}}, n) = -\operatorname{sgn}(\widetilde{D}) \frac{\partial d(a, b)}{\partial b}\bigg|_{(a,b)=(q_n(\mathbf{x}(0)), q_n(\hat{\mathbf{x}}))}. \tag{9}$$

This special reformulation allows us to interpret the weights $\widetilde{w}_t(\hat{\mathbf{x}}, b_t(\mathbf{u}))$ as weights on the pixel coordinate $\mathbf{u}$. The constant C_0 can be shown to be independent of $\mathbf{x}$. Finally, we can apply the mean-shift algorithm for the optimization of (8), as it is a weighted kernel density estimate. It is important to note that scale estimation cannot be integrated into the mean-shift optimization. To compensate for this, a heuristic scale adaptation can be applied, which runs the optimization three times with different scales. Further details can be found in [4, 13, 15].

3.4. Trust-region optimization

Alternatively, a trust-region algorithm can be applied to the optimization problem in (4). In this case, we need the gradient and the Hessian (only for the second-order algorithm) of $S(\mathbf{x})$:

$$\frac{\partial S(\mathbf{x})}{\partial \mathbf{x}}, \qquad \frac{\partial^2 S(\mathbf{x})}{\partial \mathbf{x} \partial \mathbf{x}}. \tag{10}$$

Both quantities can be derived in closed form. Due to lack of space, only the beginning of the derivation is given and the reader is referred to [13],

$$\begin{aligned}\frac{\partial S(\mathbf{x})}{\partial x_i} &= \sum_{n=1}^{N} \frac{\partial S(\mathbf{x})}{\partial q_n(\mathbf{x})} \frac{\partial q_n(\mathbf{x})}{\partial x_i} \\ &= \sum_{n=1}^{N} -\widetilde{w}_t(\mathbf{x}, n) \frac{\partial q_n(\mathbf{x})}{\partial x_i}.\end{aligned} \tag{11}$$

Note that the expression $\widetilde{w}_t(\hat{\mathbf{x}}, n)$ from the derivation of the mean-shift tracker in (9) is also required for the gradient and the Hessian (after replacing $\hat{\mathbf{x}}$ by $\mathbf{x}$). As for the mean-shift tracker, after further reformulation this expression changes into the pixel weights $\widetilde{w}_t(\hat{\mathbf{x}}, b_t(\mathbf{u}))$ (again with $\mathbf{x}$ instead of $\hat{\mathbf{x}}$). The advantage of the trust-region method consists of the ability to integrate scale and rotation estimation into the optimization problem [5, 13].

3.5. Example for mean-shift tracker

We give an example for the equations and quantities presented above. Using the Bhattacharyya distance between histograms (as in [4]),

$$D(\mathbf{q}(\mathbf{x}(0)), \mathbf{q}(\mathbf{x}(t))) = \sqrt{1 - B(\mathbf{q}(\mathbf{x}(0)), \mathbf{q}(\mathbf{x}(t)))} \quad (12)$$

with

$$B(\mathbf{q}(\mathbf{x}(0)), \mathbf{q}(\mathbf{x}(t))) = \sum_{n=1}^{N} \sqrt{q_n(\mathbf{x}(0)) \cdot q_n(\mathbf{x}(t))}, \quad (13)$$

we have $\widetilde{D}(a) = \sqrt{1-a}$, $d(a,b) = \sqrt{a \cdot b}$, and

$$\widetilde{w}_t(n) = \frac{1}{2} \sqrt{\frac{q_n(\mathbf{x}(0))}{q_n(\mathbf{x}(t))}}. \quad (14)$$

4. COMBINATION OF HISTOGRAMS

Up to now, the formulation of histogram-based tracking uses the histogram of a certain feature, defined a priori for the tracking task at hand. Examples are gray value histograms, gradient strength (edge) histograms, and RGB or HSV color histograms. Certainly, using several different features for representing the object to be tracked will result in better tracking performance, especially if the different features are weighted dynamically according to the situation in the scene. For example, a color histogram may perform badly, if illumination changes. In this case, information on the edges might be more useful. On the other hand, in case of a uniquely colored object in a highly textured environment, color is preferable over edges.

It is possible to combine several features by using one high-dimensional histogram. The problem with this approach is the curse of dimensionality; high-dimensional features result in very sparse histograms and thus a very inaccurate estimate of the true and underlying density. Instead, we propose a different solution for combining different features for object tracking. The key idea is to use a weighted combination of several low-dimensional (weighted) histograms. Let $\mathcal{H} = \{1, \ldots, H\}$ be the set of features used for representing the object. For each feature $h \in \mathcal{H}$, we define a separate function $b_t^{(h)}(\mathbf{u})$. The number of bins in histogram h is N_h and may differ between the histograms. Also, for each histogram, a different weighting function $L_{\mathbf{x}(t)}^{(h)}(\mathbf{u})$ can be applied, that is, different kernels for each individual histogram are possible if necessary. This results in H different weighted histograms $\mathbf{q}^{(h)}(\mathbf{x}(t))$ with the bins

$$q_i^{(h)}(\mathbf{x}(t)) = C_{\mathbf{x}(t)}^{(h)} \sum_{\mathbf{u} \in R(\mathbf{x}(t))} L_{\mathbf{x}(t)}^{(h)}(\mathbf{u}) \delta(b_t^{(h)}(\mathbf{u}) - i), \quad h \in \mathcal{H},\ i = 1, \ldots, N_h. \quad (15)$$

We now define a combined representation of the object by $\phi(\mathbf{x}(t)) = (\mathbf{q}^{(h)}(\mathbf{x}(t)))_{h \in \mathcal{H}}$ and a new distance function (compare (4) and (5)), based on the weighted sum of the distances for the individual histograms,

$$D^*(\mathbf{x}) = \sum_{h \in \mathcal{H}} \beta_h D_h(\mathbf{q}^{(h)}(\mathbf{x}(0)), \mathbf{q}^{(h)}(\mathbf{x}(t))), \quad (16)$$

where $\beta_h \geq 0$ is the contribution of the individual histogram h to the object representation. The quantities β_h can be adjusted to best model the object in the current context of tracking. In Section 5, we will present a mechanism for online adaptation of the feature weights. Alternatively, instead of the linear combination $D^*(\mathbf{x})$ of the distances $D_h(\mathbf{q}^{(h)}(\mathbf{x}(0)), \mathbf{q}^{(h)}(\mathbf{x}(t)))$, a linear combination of the simplified expressions $S_h(\mathbf{x})$ (straight forward generalization of (7)) can be used as follows:

$$S^*(\mathbf{x}) = \sum_{h \in \mathcal{H}} \beta_h S_h(\mathbf{x}(t)). \quad (17)$$

In the single histogram case, minimizing $D(\mathbf{q}(\mathbf{x}(0)), \mathbf{q}(\mathbf{x}(t)))$ is equivalent to minimizing $S(\mathbf{x})$. In the combined histogram case, however, the equivalence of minimizing $D^*(\mathbf{x})$ and $S^*(\mathbf{x})$ can only be guaranteed, if $\widetilde{D}_h(a) = \pm a$ for all $h \in \mathcal{H}$. Nevertheless, $S^*(\mathbf{x})$ can still be used as an objective function, if this condition is not fulfilled. Because of its simpler form and the lack of obvious advantages of $D^*(\mathbf{x})$, we choose the following optimization problem for the combined histogram tracker:

$$\mathbf{x}(t) = \operatorname*{argmax}_{\mathbf{x}} S^*(\mathbf{x}). \quad (18)$$

From a theoretical point of view, using the simplified objective function S^* is equivalent to restricting the class of distance measures D_h for each feature h to those that fulfill $\widetilde{D}_h(a) = \pm a$ (as in this case $D_h = S_h$). For example, this excludes the Euclidean distance, but does allow for the squared Euclidean distance.

4.1. Mean-shift optimization

For the mean-shift tracker, we have to use the same weighting function $L_{\mathbf{x}(t)}(\mathbf{u})$ for all histograms h and again the state $\mathbf{x}$ has to be restricted to the position of the moving object in the image plane. After a technically somewhat tricky, but conceptually straight forward extension of the derivation for the single histogram mean-shift tracker, we get

$$\mathbf{x}(t) \approx \operatorname*{argmax}_{\mathbf{x}} C_0 \sum_{\mathbf{u} \in R(\mathbf{x})} L_{\mathbf{x}}(\mathbf{u}) \underbrace{\sum_{h \in \mathcal{H}} \widetilde{w}_{h,t}(\hat{\mathbf{x}}, b_t^{(h)}(\mathbf{u}))}_{:= w_t(\hat{\mathbf{x}}, \mathbf{u})}, \quad (19)$$

which is again a weighted kernel density estimate. The corresponding pixel weights are

$$w_t(\hat{\mathbf{x}}, \mathbf{u}) = \sum_{h \in \mathcal{H}} \widetilde{w}_{h,t}(\hat{\mathbf{x}}, b_t^{(h)}(\mathbf{u})) = \sum_{h \in \mathcal{H}} -\beta_h \operatorname{sgn}(D_h) \frac{\partial d_h(a,b)}{\partial b} \Big|_{(a,b) = (q_{b_t(\mathbf{u})}^{(h)}(\mathbf{x}(0)), q_{b_t(\mathbf{u})}^{(h)}(\hat{\mathbf{x}}))}, \quad (20)$$

where $d_h(a,b)$ is defined as in (5) for each individual feature h.

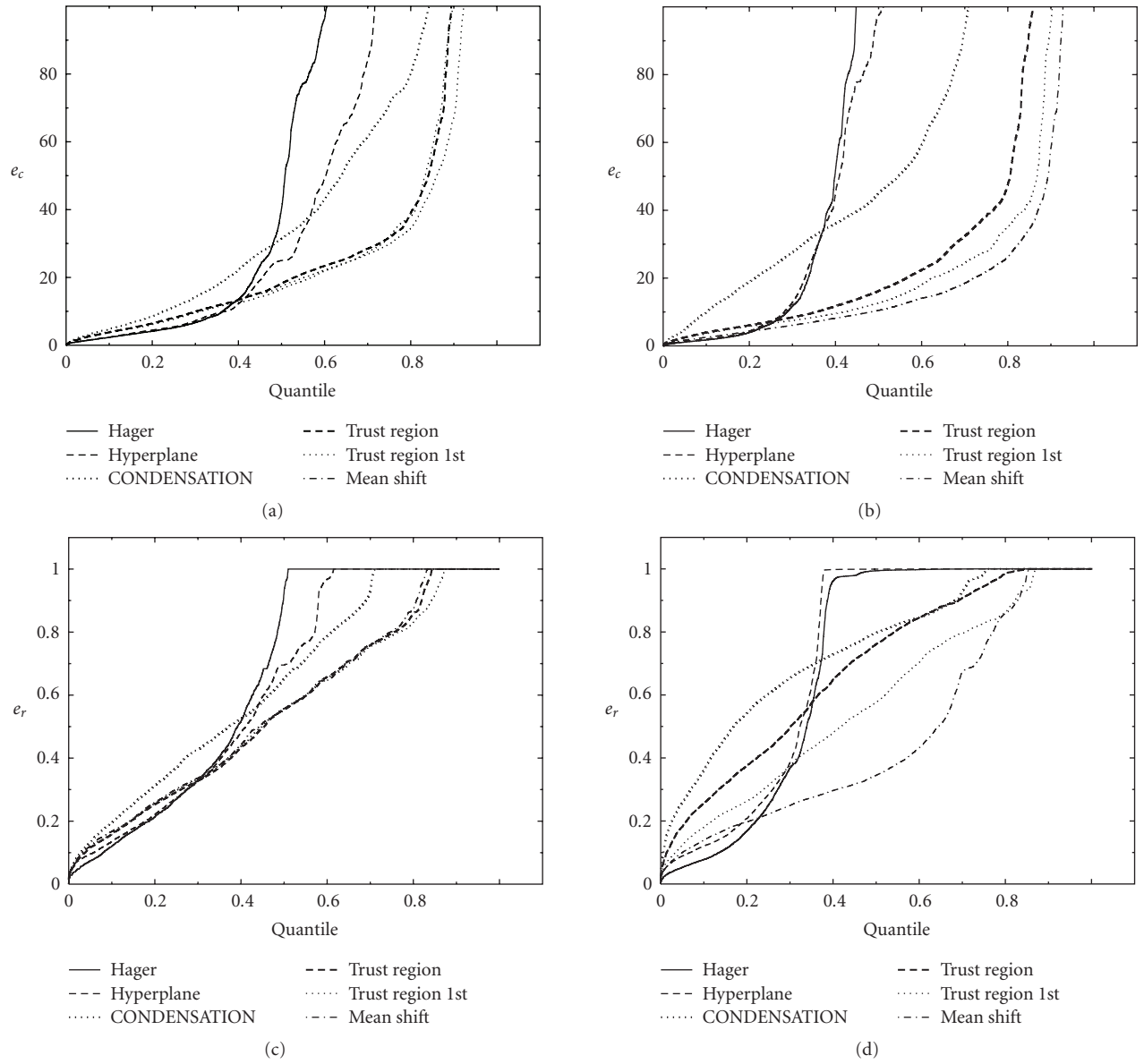

Figure 1: The result graphs for the tracker comparison experiments. The top row shows the distance error e_c, the bottom row shows the region error e_r. The left-hand column contains the results for trackers without scale estimation, the right-hand column those with scale estimation. The horizontal axis does not correspond to time, but to sorted aggregation over all test videos. In other words, each graph shows "all" error quantiles (also known as percentiles). The vertical axis for e_c has been truncated to 100 pixels to emphasize the relevant details.

4.2. Trust-region optimization

For the trust-region optimization, again the gradient and the Hessian of the objective function have to be derived. As the simplified objective function $S^*(\mathbf{x})$ is a linear combination of the simplified distance measures $S_h(\mathbf{x})$ for the individual histograms h, the gradient of $S^*(\mathbf{x})$) is a linear combination of the gradient in the single histogram case $S_h(\mathbf{x})$,

$$\frac{\partial S^*(\mathbf{x})}{\partial x_i} = \frac{\partial}{\partial x_i}\left(\sum_{h\in\mathcal{H}} \beta_h S_h(\mathbf{x})\right) = \sum_{h\in\mathcal{H}} \beta_h \frac{\partial S_h(\mathbf{x})}{\partial x_i}, \tag{21}$$

The same applies to the Hessian,

$$\begin{aligned}\frac{\partial^2 S^*(\mathbf{x})}{\partial x_j \partial x_i} &= \frac{\partial}{\partial x_j}\left(\frac{\partial S^*(\mathbf{x})}{\partial x_i}\right)\\ &= \frac{\partial}{\partial x_j}\left(\sum_{h\in\mathcal{H}} \beta_h \frac{\partial S_h(\mathbf{x})}{\partial x_i}\right)\\ &= \sum_{h\in\mathcal{H}} \beta_h \frac{\partial}{\partial x_j}\left(\frac{\partial S_h(\mathbf{x})}{\partial x_i}\right).\end{aligned} \tag{22}$$

The factor $\partial S_h(\mathbf{x})/\partial x_i$ is the ith component of the gradient in the single histogram case. The factor $\partial/\partial x_j(\partial S_h(\mathbf{x})/\partial x_i)$ is the entry (i, j) of the Hessian in the single histogram case. Details can be found in [13].

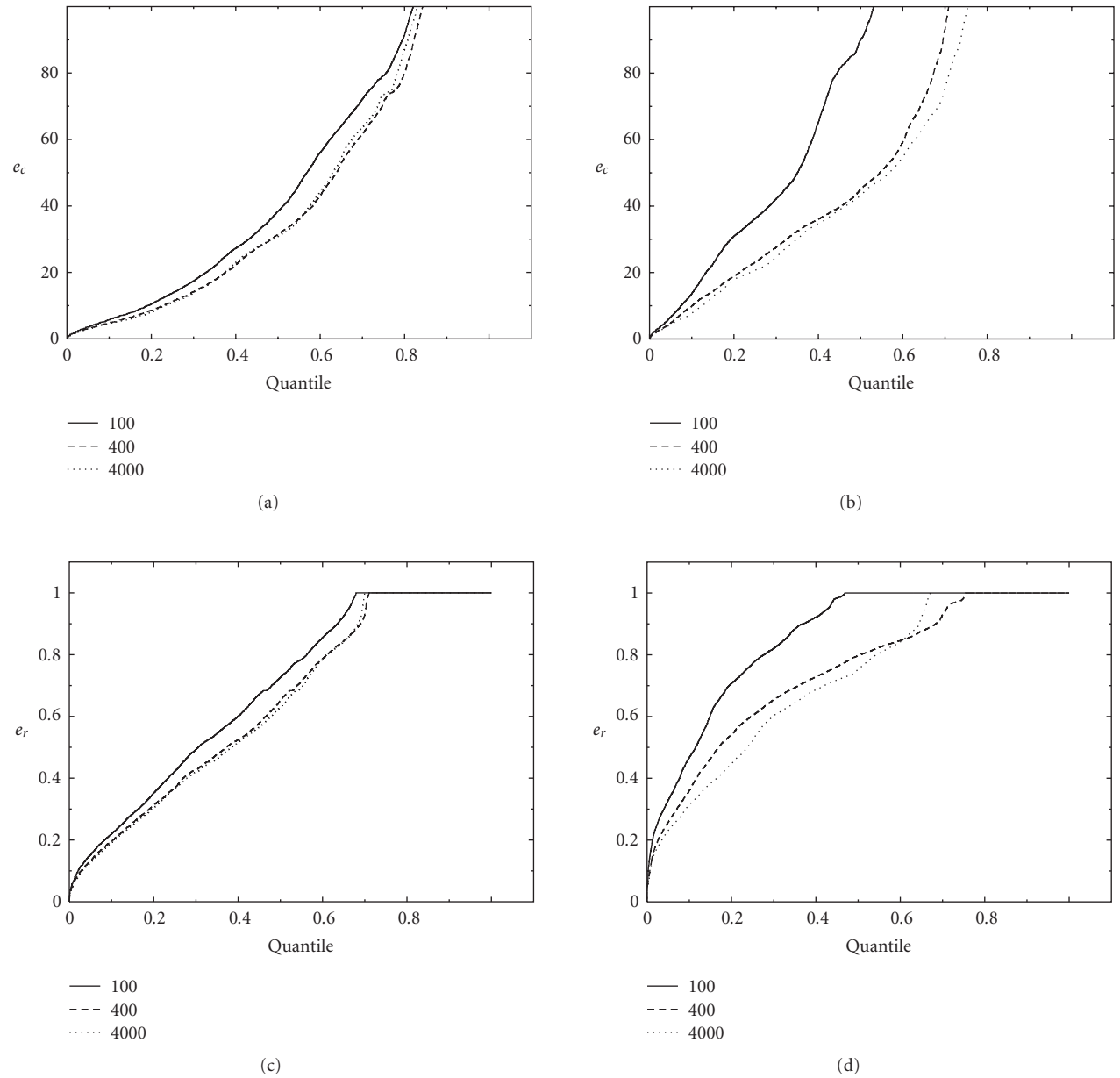

Figure 2: Same evaluation as in Figure 1 for three configurations of the CONDENSATION tracker with different numbers of particles.

Note that for the trust-region trackers, the simplification of the objective function D^* to S^* is not necessary. However, without the simplification, the gradient and the Hessian of the objective function $D^*(\mathbf{x})$ are *no longer* linear combinations of the gradient and the Hessian for the full single histogram distance measures D_h and thus the resulting expressions are more complicated and computationally more expensive—without an obvious advantage. Note also, that for the case of a common kernel for all features, the difference between the single histogram and the multiple histogram case is that the expression $\widetilde{w}_t(\mathbf{x}, n)$ is replaced by $w_t(\mathbf{x}, n)$, which is the same expression as for the combined histogram mean-shift tracker (see Sections 3.4 and 4.1).

5. ONLINE ADAPTATION OF FEATURE WEIGHTS

As described in Section 4, the feature weights $\beta_h, h \in \mathcal{H}$ are constant throughout the tracking process. However, the most discriminative feature combination can vary over time. For example, as the object moves, the surrounding background can change drastically, or motion blur can have a negative influence on edge features for a limited period of time. Several authors have proposed online feature selection mechanisms for tracking. They either select one feature [16] or several features which they combine empirically *after* performing tracking with each winning feature [17, 18]. A further approach computes an "artificial" feature using

principal component analysis [19]. Democratic integration [20], on the other hand, assigns a weight to each feature and adapts these weights based on the recent performance of the individual features. Given our combined histogram tracker (CHT), we follow the idea of dynamically adapting the weight β_h of each individual feature h. To emphasize this, we use the notation $\beta_h(t)$ in this section. Unlike Democratic Integration, we perform weight adaptation in an explicit and very efficient tracking framework.

The central part of feature selection as well as adaptive weighting is a measure for the tracking performance of each feature. Typically, the discriminability between object and surrounding background is estimated for each feature. In our case, this quality measure is used to increase the weights of good features and decrease the weights of bad features. In the context of this work, a natural choice for such a quality measure is the distance,

$$\rho_h(t) = D_h\left(\mathbf{q}^{(h)}(\mathbf{x}(t)), \mathbf{p}^{(h)}(\mathbf{x}(t))\right), \tag{23}$$

between the object histogram $\mathbf{q}^{(h)}(\mathbf{x}(t))$ and the histogram $\mathbf{p}^{(h)}(\mathbf{x}(t))$ of an area surrounding the object ellipse. Both histograms are extracted *after* tracking in frame t. We apply three different weight adaptation strategies.

(1) The weight of the feature h with the best quality $\rho_h(t)$ is increased by multiplying with a factor γ (set to 1.3),

$$\beta_h(t+1) = \gamma\beta_h(t). \tag{24}$$

Accordingly, the feature h' with the worst quality $\rho_{h'}(t)$ is decreased by dividing by γ,

$$\beta_{h'}(t+1) = \frac{\beta_{h'}(t)}{\gamma}. \tag{25}$$

Upper and lower limits are imposed on β_h for every feature h to keep weights from diverging. We used the bounds 0.01 and 100. This adaptation strategy is only suited for two features ($H = 2$).

(2) The weight $\beta_h(t+1)$ of each feature h is set to its quality measure $\rho_h(t)$,

$$\beta_h(t+1) = \rho_h(t). \tag{26}$$

(3) The weight $\beta_h(t+1)$ of each feature h is slowly adapted toward $\rho_h(t)$ using a convex combination (IIR filter) with parameter ν (set to 0.1 in our experiments),

$$\beta_h(t+1) = \nu\rho_h(t) + (1-\nu)\beta_h(t). \tag{27}$$

6. EXPERIMENTAL EVALUATION

6.1. Test set and evaluation criteria

In the experiments, we use some of the test videos of the CAVIAR project [7], originally recorded for action and behavior recognition experiments. The videos are perfectly suited, since they are recorded in a "natural" environment, with change in illumination and scale of the moving persons as well as partial occlusions. Most importantly, the moving persons are hand-labelled, that is, for each frame, a ground truth rectangle is stored. In case of the mean-shift and trust-region trackers, the ground truth rectangles are transformed into ellipses to avoid systematic errors in the tracker evaluation based on (27).

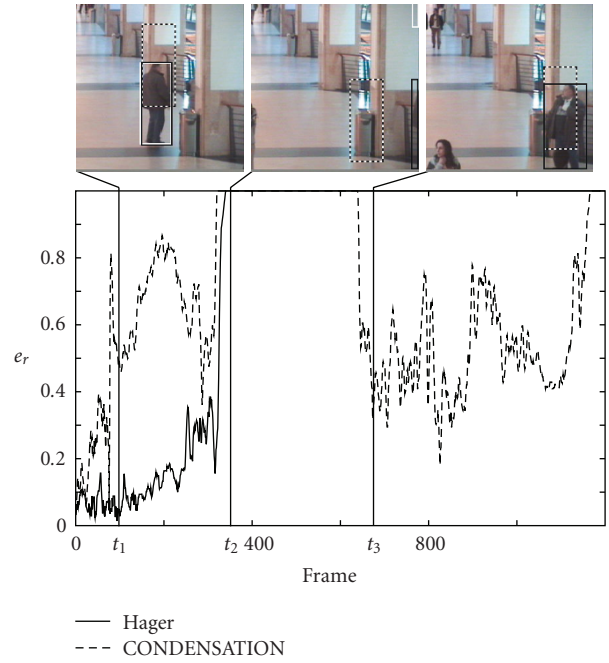

Figure 3: Comparison of the Hager and CONDENSATION trackers using the e_r error measure (28). The black rectangle shows the ground truth. The white rectangle is from the Hager tracker, the dashed rectangle from the CONDENSATION tracker. The top, middle, and bottom images are from frames t_1, t_2, and t_3, respectively. The tracked person (almost) leaves the camera's field of view in the middle image, and returns shortly before time t_3. The Hager tracker is more accurate, but loses the person irretrievably, while the CONDENSATION tracker is able to reacquire the person.

In each experiment, a specific person was tracked. The tracking system was given the frame number of the first unoccluded appearance of the person, the accordant ground truth rectangle around the person as initialization, and the frame of the person's disappearance. Aside from this initialization, the trackers had no access to the ground truth information. Twelve experiments were performed on seven videos (some videos were reused, tracking a different person each time).

To evaluate the results of the original trackers as well as our extensions, we used an area-based criterion. We measure the difference e_r of the region A computed by the tracker and the ground-truth region B,

$$e_r(A,B) := \frac{|A \setminus B| + |B \setminus A|}{|A| + |B|} = 1 - \frac{|A \cap B|}{1/2(|A| + |B|)}, \tag{28}$$

where $|A|$ denotes the number of pixels in region A. This error measure is zero if the two regions are identical, and one if they do not overlap. If the two regions have the same size, the error increases with increasing distance between the

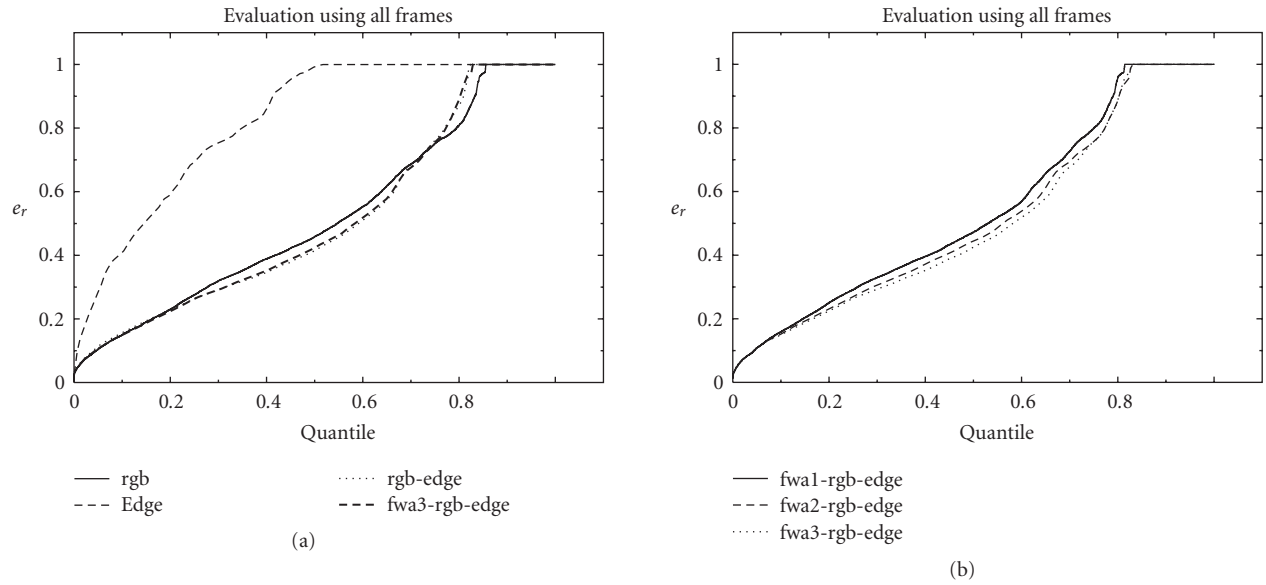

Figure 4: Sorted error (i.e., all quantiles as in Figure 1) using CHT with RGB and gradient strength with constant weights (*rgb-edge*) and three different feature weight adaptation mechanisms (*fwa1-rgb-edge*, *fwa2-rgb-edge*, and *fwa3-rgb-edge*), as well as single histogram trackers using RGB (*rgb*) and edge histogram (*edge*). Results are given for the mean-shift tracker with scale estimation, Biweight-Kernel, and Kullback-Leibler distance for all individual histograms.

center of both regions. Equal centers but different sizes are also taken into account. We also compare the trackers using the Euclidean distance e_c between the centers of A and B.

6.2. General comparison

In the first part of the experiments, we give a general comparison of the following six trackers, which were tested with pure translation estimation, as well as with translation and scale estimation.

(i) The region tracking algorithm of Hager and Belhumeur [2], working on a three-level Gaussian image pyramid to enlarge the basin of convergence.

(ii) The hyperplane tracker, using a 150-point region and initialized with 1000 training perturbation steps.

(iii) The mean-shift and two trust-region algorithms, using an Epanechnikov weighting kernel, the Bhattacharyya distance measure, and the HSV color histogram feature introduced by Pérez et al. [6] for maximum comparability.

(iv) Finally, the CONDENSATION-based color histogram approach of Pérez et al. [6]. As this tracker is computationally expensive, we choose only 400 particles for the main comparison, and alternatively 100 and 4000. Furthermore, we kept the particle size as low as possible: two position parameters and an additional scale parameter if applicable. The algorithm is thus restricted to a simplified motion model, which estimates the velocity of the object by taking the difference between the position estimates from the last two frames. The predicted particles are diffused by a zero-mean Gaussian distribution with a variance of 5 pixels in each dimension.

These experiments were timed on a 2.8 GHz Intel Xeon processor. The methods differ greatly in the time taken for initialization (once per sequence) and tracking (once per frame). Table 1 shows the results for the first sequence. Note the long initialization of the hyperplane tracker due to training, and the long per-frame time of the CONDENSATION.

Table 1: Timing results for the first sequence, in milliseconds. For each tracker, the time taken for initialization and the average time per frame are shown with and without scale estimation.

	Without scale		With scale	
	Initial	Per frame	Initial	Per frame
Hager	4	2.40	5	2.90
Hyperplane	557	2.22	548	2.21
Mean shift	2	1.04	2	2.75
Trust region	9	4.01	18	8.63
Trust region 1st	5	7.25	6	12.09
CONDENSATION 100	11	27.71	11	40.50
CONDENSATION 400	11	79.67	11	109.85
CONDENSATION 4000	14	706.62	14	962.02

For each tracker, the errors e_c and e_r from all sequences were concatenated and sorted. Figure 1 shows the measured distance error e_c and the region error e_r for all trackers, with and without scale estimation. Performance varies widely between all tested trackers, showing strengths and weaknesses of each individual method. There appears to be no method which is universally "better" than the others.

The structure-based region trackers, Hager and hyperplane, are potentially very accurate, as can be seen at the left-hand side of each graph, where they display a larger number of frames with low errors. However, both are prone to losing the target rather quickly, causing their errors to climb faster

than the other three methods. Particularly when scale is also estimated, the additional degree of freedom typically provides additional accuracy, but causes the estimation to diverge sooner. This is due to strong appearance changes of the tracked regions in these image sequences.

The CONDENSATION method, for the most part, is not as accurate as the three local optimization methods: mean-shift and the two trust-region variants. Figure 2 shows the performance with three different numbers of particles, the severe influence on computation times can be seen in Table 1. As expected, increasing the number of particles improves the tracking results. However, the relative performance in comparison with the other trackers is mostly unaffected. We believe that this is partly due to the fact that time constraints necessitate the use of a quickly computable particle evaluation function, which does *not* include a spatial kernel—in contrast to the other histogram-based methods.

Figure 3 shows a direct comparison between a locally optimizing structural tracker (Hager) and the globally optimizing histogram-based CONDENSATION tracker. It is clearly visible that the Hager tracker provides more accurate results, but cannot reacquire a lost target. The CONDENSATION tracker, on the other hand, can continue to track the person after it reappears.

The mean-shift and both trust-region trackers show a very similar performance and provide the best overall tracking if scale estimation is turned off. With scale estimation, however, the mean-shift algorithm performs noticeably better than the first-order trust-region approach, which in turn is better than second-order trust-region tracker. This is especially visible when comparing the region error e_r (Figure 1(d)), where the error in the scale component plays an important role. This is probably caused by the very different approaches to scale estimation in the two types of trackers. While the trust-region trackers directly incorporate scale estimation with variable aspect ratio into the optimization problem, the mean-shift tracker uses a heuristic approach which limits the maximum scale change per frame (to 1% in our experiments [4, 13]). It seems that this forcedly slow scale adaptation keeps the mean-shift tracker from over adapting the scale to changes in object and/or background appearance. The first-order trust-region tracker seems to benefit from the fact that its first-order optimization algorithm has *worse* convergence properties than the second-order variant, which seems to reduce the scale over adaption of the scale parameters.

Another very interesting aspect to note is that tracking translation and scale, as opposed to tracking translation only, does *not* generally improve the results of most trackers. The two template trackers gain a little extra precision, but lose the object much earlier. The changing appearance of the tracked persons is a strong handicap for them as the image constancy assumption is violated. The additional degree of freedom opens up more chances to diverge toward local optima, which causes the target to be lost sooner. The mean-shift tracker does actually perform better with scale estimation. The other histogram-based trackers are better in case of pure translation estimation. They suffer from the fact that the features themselves are typically rather invariant under scale changes. Once the scale is wrong, small translations of the target can go completely unnoticed.

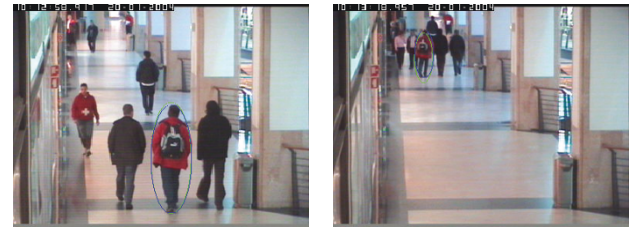

(a) (b)

Figure 5: Tracking results for one of the CAVIAR images sequences (first and last image of the successfully tracked person). The tracking results are almost identical to the ground truth regions (ellipses). Note the scale change of the person between the two images.

6.3. Improvements of the combined histogram tracker

In the second part of the experiments, we combined two different histograms. The first is the standard color histogram consisting of the RGB channels, abbreviated in the figures as *rgb*. The second histogram is computed from a Sobel edge strength image (*edge*), with the edge strength normalized to fit the gray-value range from 0 to 255.

In Figure 4, the tracking accuracy of the mean-shift tracker is shown. The graph displays the error e_r accumulated and sorted over all sequences (same scheme as in Figure 1). In other words, the graph shows "all" error quantiles. The reader can verify that a combination of RGB and gradient strength histograms leads to an improvement of tracking accuracy compared to a pure RGB histogram tracker, even though the object is lost a bit earlier. We got similar results for the corresponding trust-region tracker with our extension to combined histograms. The weights β_h for combining RGB and edge histograms (compare (16)) have been empirically set to 0.8 and 0.2. The computation time for one image is on average approximately 2 milliseconds on a 3.4 GHz P4 compared to approximately 1 millisecond for a tracker using one histogram only. A successful tracking example including correct scale estimation is shown in Figure 5.

6.4. Improvements with weight adaptation

In the third part of the experiments, we evaluate the performance of the CHT with weight adaptation. We include the three feature weight adaptation mechanisms (*fwa1, fwa2, fwa3* according to the numbers in Section 5) in the experiment of Section 6. All adaptation mechanisms are initialized with both feature weights set to 0.5. Results are given in Figure 4. The third weight adaptation mechanism (*fwa3-rgb-edge*) performs almost as good as the manually optimized constant weights (*rgb-edge*). Figure 4(b) gives a comparison of the three feature weight adaptation mechanisms. Here, the third adaptation mechanism gives the best results.

As the RGB histogram dominates the gradient strength histogram, we use the blue- and green color channels as

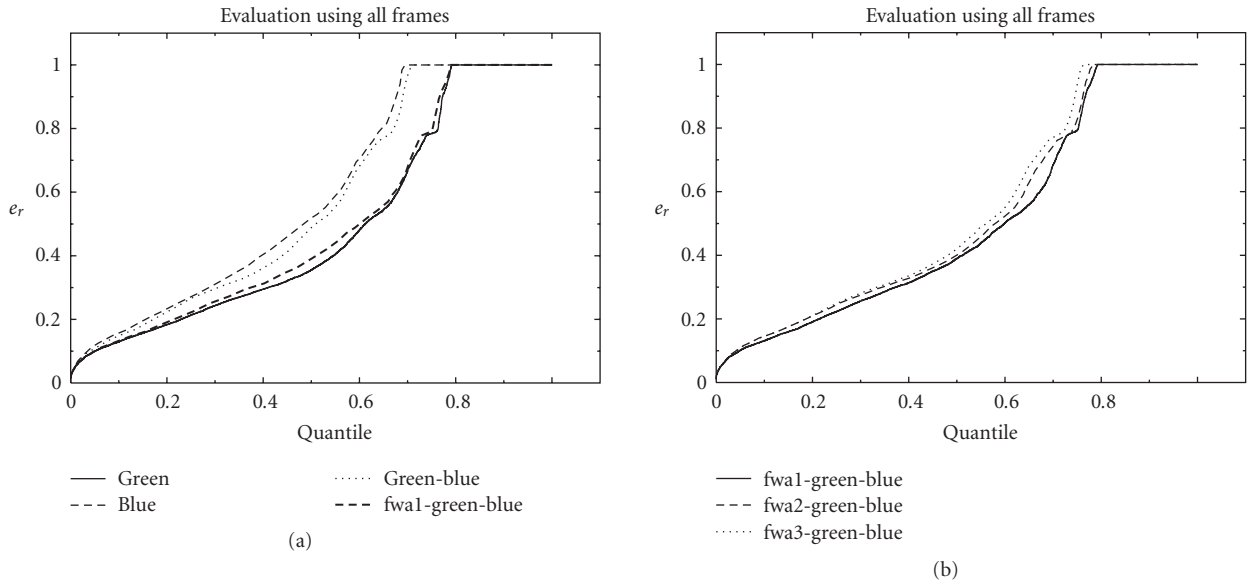

Figure 6: Sorted error (i.e., all quantiles as in Figure 1) using CHT with green and blue histograms with constant weights (*green-blue*) and three different feature weight adaptation mechanisms (*fwa1-green-blue, fwa2-green-blue, and fwa3-green-blue*), as well as single histogram trackers using a green (*green*) and a blue histogram (*blue*). Results are given for the mean-shift tracker with scale estimation, biweight-kernel, and Kullback-Leibler distance for all individual histograms.

individual features in the second experiment. Both feature weights are set to 0.5 for the CHT with and without weight adaptation. All other parameters are kept as in the previous experiment. The results are displayed in Figure 6. The single histogram tracker using the green feature performs better than the blue feature. The CHT gives similar results to the blue feature, which is caused by bad feature weights. With weight adaptation, the performance of the CHT is greatly improved and almost reaches that of the green feature. This shows that, even though the single histogram tracker with the green feature gives the best results, the CHT with weight adaptation performs almost equally well *without a good initial guess* for the best single feature or the best constant feature weights. Figure 6(b) gives a comparison of the three feature weight adaptation mechanisms. Here, the first adaptation mechanism gives the best results. The average computation time for one image is approximately 4 milliseconds on a 3.4 GHz P4 compared to approximately 2 milliseconds for the CHT with constant weights.

7. CONCLUSIONS

As the first contribution of this paper, we presented a comparative evaluation of five state-of-the-art algorithms for data-driven object tracking, namely Hager's region tracking technique [2], Jurie's hyperplane approach [3], the probabilistic color histogram tracker of Pérez et al. [6], Comaniciu's mean-shift tracking approach [4], and the trust-region method introduced by Liu and Chen [5]. All of those trackers have the ability to estimate the position and scale of an object in an image sequence in real-time. The comparison was carried out on part of the CAVIAR video database, which includes ground-truth data. The results of our experiments show that, in cases of strong appearance change, the template-based methods tend to lose the object sooner than the histogram-based methods. On the other hand, if the appearance change is minor, the template-based methods surpass the other approaches in tracking accuracy. Comparing the histogram-based methods among each other, the mean-shift approach [4] leads to the best results. The experiments also show that the probabilistic color histogram tracker [6] is not quite as accurate as the other techniques, but is more robust in case of occlusions and appearance changes. Note, however, that the accuracy of this tracker depends on the number of particles, which has to be chosen rather small to achieve real-time precessing.

As the second contribution of our paper, we presented a mathematically consistent extension of histogram-based tracking, which we call combined histogram tracker (CHT). We showed that the corresponding optimization problems can still be solved using the mean-shift as well as the trust-region algorithms without loosing real-time capability. The formulation allows for the combination of an arbitrary number of histograms with different dimensions and sizes, as well as individual distance functions for each feature. This allows for high flexibility in the application of the method.

In the experiments, we showed that a combination of two features can improve tracking results. The improvement of course depends on the chosen histograms, the weights, and the object to be tracked. We would like to stress again that similar results were achieved using the trust-region algorithm, although the presentation in this paper was focused on the mean-shift algorithm. For more details, the reader is referred to [13]. We also presented three online weight adaptation mechanisms for the combined histogram tracker. The benefit of feature weight adaptation is that an

initial choice of a single best feature or optimal combination weights is no longer necessary, as has been shown in the experiments. One important result is that the CHT with (and also without) weight adaptation can still be applied in real-time on standard PC hardware.

In our future work, we will evaluate the performance of the weight adaptation mechanisms on more than two features and investigate more sophisticated adaptation mechanisms. We are also going to systematically compare the CHT with the other trackers described in this paper.

ACKNOWLEDGMENTS

This work was partially funded by the German Science Foundation (DFG) under grant SFB 603/TP B2. This work was partially funded by the European Commission 5th IST Programme—Project VAMPIRE.

REFERENCES

[1] B. Deutsch, Ch. Gräßl, F. Bajramovic, and J. Denzler, "A comparative evaluation of template and histogram based 2D tracking algorithms," in *Proceedings of the 27th Annual Meeting of the German Association for Pattern Recognition (DAGM '05)*, pp. 269–276, Vienna, Austria, August-September 2005.

[2] G. D. Hager and P. N. Belhumeur, "Efficient region tracking with parametric models of geometry and illumination," *IEEE Transactions on Pattern Analysis and Machine Intelligence*, vol. 20, no. 10, pp. 1025–1039, 1998.

[3] F. Jurie and M. Dhome, "Hyperplane approach for template matching," *IEEE Transactions on Pattern Analysis and Machine Intelligence*, vol. 24, no. 7, pp. 996–1000, 2002.

[4] D. Comaniciu, V. Ramesh, and P. Meer, "Kernel-based object tracking," *IEEE Transactions on Pattern Analysis and Machine Intelligence*, vol. 25, no. 5, pp. 564–577, 2003.

[5] T.-L. Liu and H.-T. Chen, "Real-time tracking using trust-region methods," *IEEE Transactions on Pattern Analysis and Machine Intelligence*, vol. 26, no. 3, pp. 397–402, 2004.

[6] P. Pérez, C. Hue, J. Vermaak, and M. Gangnet, "Color-based probabilistic tracking," in *Proceedings of the 7th European Conference on Computer Vision (ECCV '02)*, vol. 1, pp. 661–667, Copenhagen, Denmark, May 2002.

[7] CAVIAR, EU funded project, IST 2001 37540, 2004, http://homepages.inf.ed.ac.uk/rbf/CAVIAR.

[8] F. Bajramovic, Ch. Gräßl, and J. Denzler, "Efficient combination of histograms for real-time tracking using mean-shift and trust-region optimization," in *Proceedings of the 27th Annual Meeting of the German Association for Pattern Recognition (DAGM '05)*, pp. 254–261, Vienna, Austria, August-September 2005.

[9] Cheng, "Mean shift, mode seeking, and clustering," *IEEE Transactions on Pattern Analysis and Machine Intelligence*, vol. 17, no. 8, pp. 790–799, 1995.

[10] A. R. Conn, N. I. M. Gould, and P. L. Toint, *Trust-Region Methods*, SIAM, Philadelphia, Pa, USA, 2000.

[11] S. Baker, R. Gross, and I. Matthews, "Lucas-Kanade 20 years on: a unifying framework: part 4," Tech. Rep. CMU-RI-TR-04-14, Robotics Institute, Carnegie Mellon University, Pittsburgh, Pa, USA, 2004.

[12] M. P. Wand and M. C. Jones, *Kernel Smoothing*, Chapman & Hall/CRC, Boca Raton, Fla, USA, 1995.

[13] F. Bajramovic, *Kernel-basierte Objektverfolgung*, M.S. thesis, Computer Vision Group, Department of Mathematics and Computer Science, University of Passau, Lower Bavaria, Germany, 2004.

[14] M. Isard and A. Blake, "CONDENSATION—conditional density propagation for visual tracking," *International Journal of Computer Vision*, vol. 29, no. 1, pp. 5–28, 1998.

[15] D. Comaniciu and P. Meer, "Mean shift: a robust approach toward feature space analysis," *IEEE Transactions on Pattern Analysis and Machine Intelligence*, vol. 24, no. 5, pp. 603–619, 2002.

[16] H. Stern and B. Efros, "Adaptive color space switching for tracking under varying illumination," *Image and Vision Computing*, vol. 23, no. 3, pp. 353–364, 2005.

[17] R. T. Collins, Y. Liu, and M. Leordeanu, "Online selection of discriminative tracking features," *IEEE Transactions on Pattern Analysis and Machine Intelligence*, vol. 27, no. 10, pp. 1631–1643, 2005.

[18] B. Kwolek, "Object tracking using discriminative feature selection," in *Proceedings of the 8th International Conference on Advanced Concepts for Intelligent Vision Systems (ACIVS'06)*, pp. 287–298, Antwerp, Belgium, September 2006.

[19] B. Han and L. Davis, "Object tracking by adaptive feature extraction," in *Proceedings of the International Conference on Image Processing (ICIP '04)*, vol. 3, pp. 1501–1504, Singapore, October 2004.

[20] J. Triesch and C. von der Malsburg, "Democratic integration: self-organized integration of adaptive cues," *Neural Computation*, vol. 13, no. 9, pp. 2049–2074, 2001.